Research Article

Efficient Inverted Perovskite Solar Cells Enabled by Dopant-Free Hole-Transporting Materials Based on Dibenzofulvene-Bridged Indacenodithiophene Core Attaching Varying Alkyl Chains

Enwei Zhu,[†] Jiantao Wang,[†] Jing Xu, Liying Fu, Ruxue Li, Chengzhuo Yu, Shijie Ge, Xiaosong Lin, Rui Chen, Hongkai Wu, Hsing-lin Wang,* and Guangbo Che*

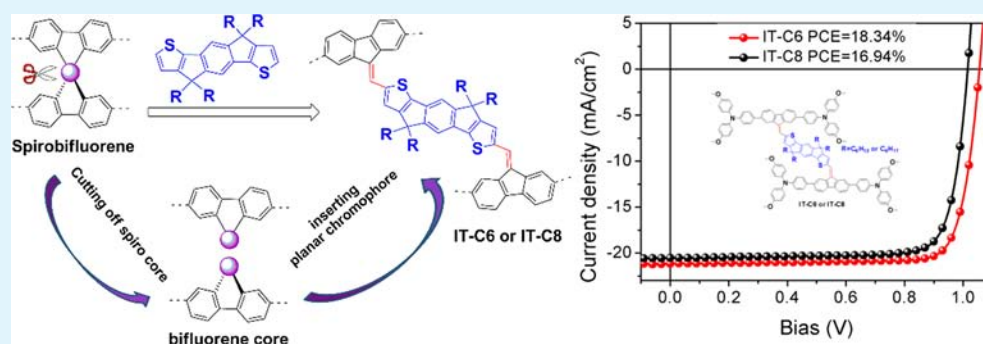Cite This: ACS Appl. Mater. Interfaces 2021, 13, 13254−13263

Read Online

ACCESS | Metrics & More | Article Recommendations | SI Supporting Information

ABSTRACT: Inspired by the structural advantages of spiro-OMeTAD, which is the most commonly used hole-transporting material (HTM), two rationally designed HTMs with butterfly-shaped triarylamine groups based on dibenzofulvene-bridged indacenodithiophene (IDT) core (attaching hexyl and octyl chains) have been synthesized, namely, IT-C6 and IT-C8, respectively. Shorter alkyl-chain-based IT-C6 exhibits a marked increase in glass-transition temperature (T_g) of 105 °C, whereas IT-C8 shows a T_g of 95 °C. Moreover, it is demonstrated that IT-C6 exhibits a higher hole-transporting mobility, more suitable band energy alignment, better interfacial contact, and passivation effect. The inverted devices of employed HTM based on IT-C6 obtained a champion PCE of 18.34% with a remarkable fill factor (FF) of 82.32%, whereas the IT-C8-based device delivered an inferior PCE of 16.94% with an FF up to 81.20%. Both HTMs embodied inverted devices present high FF values greater than 81%, which are among the highest reported values of small molecular HTM-based PSCs. This work reveals that cutting off the symmetrical spiro-core and subsequently combining IDT (attaching tailored alkyl chains) with the spiro-linkage fluorine to construct the orthogonal molecular conformation is a significant principle for the design of promising dopant-free HTMs.

KEYWORDS: perovskite solar cells, hole-transporting materials, dopant-free, dibenzofulvene-bridged indacenodithiophene core, fill factor

1. INTRODUCTION

Perovskite solar cells (PSCs) have become a power competitor in new-generation photovoltaics because of the rapid developing power conversion efficiency (PCE) and low-cost raw materials and solution processing techniques.[1,2] Two main architectures of PSCs, regular (mesoporous and n-i-p) and inverted (p-i-n), have been dominantly investigated, wherein the regular device gained a PCE as high as 25.5% but suffered from poor stability, whereas the inverted structure achieved stable operation in spite of relatively low PCE (certified 22.75%).[3−5] In a typical device architecture, hole-transporting materials (HTMs), sandwiched between perovskite and anode, play a critical role in realizing the highest tandem device performance (29.1%) and long-term stability.[6−8] To date, the most commonly used small molecular HTM is 2,2′,7,7′-tetrakis(N,N-dipmethoxyphenylamine)-9,9′-spirobifluorene (spiro-OMeTAD) featuring twisted spiro-bifluorene core-

linked triphenylamine (TPA) moieties via orthogonal molecular conformation.[9,10] The TPA as the preferential hole-transporting moiety in spiro-OMeTAD should lead to weak intermolecular interactions induced by the orthogonal molecular conformation that suppresses the forming of intermolecular $\pi-\pi$ stacking, which limits the hole-transport mobility.[11−13] Due to low intrinsic hole-mobility of spiro-OMeTAD, the high-efficiency PSCs should be achieved with the assistance of dopants when fabricating HTM films.[14,15]
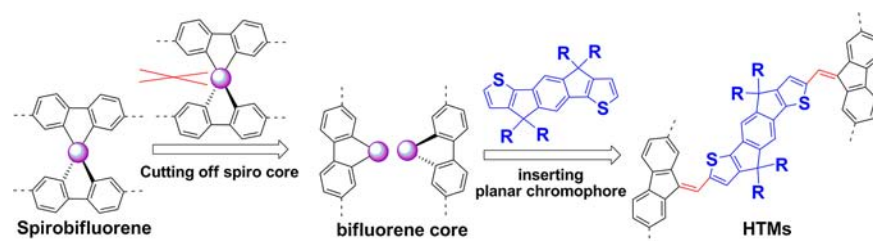
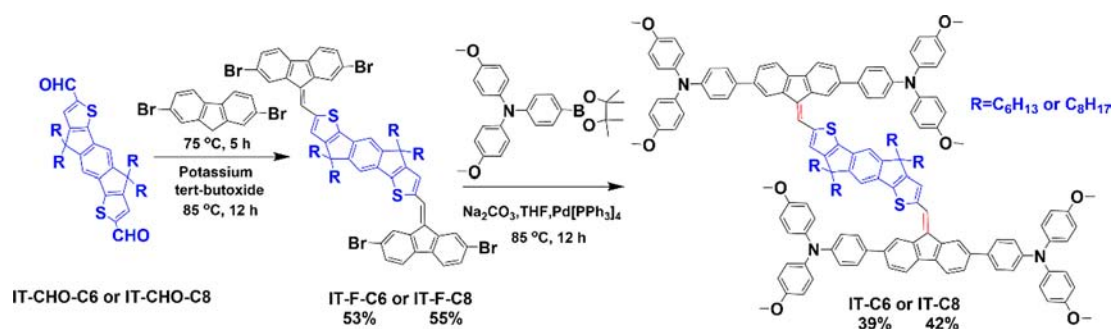**Scheme 1. Molecular Design Idea and Target Framework of Small Molecular HTMs**

Scheme 2. Synthetic Routes of Small Molecular HTMs

However, this wide introduction of dopants not only results in more complex device fabrication and rapid deterioration of the device but also induces additional production costs.[16,17] Therefore, from the view of molecular design, replacement of the orthogonal spiro core of spiro-OMeTAD with planar conjugated building blocks is desired to obtain high-charge-mobility HTM without dopants.

Indacenodithiophene (IDT) as an essential fused-ring central core has been widely employed to construct the A-D-A type nonfullerene acceptors for highly efficient organic solar cells.[18−20] The extended aromatic π-conjugation of coplanar fused-ring IDT and the easy polarization of sulfur atom containing in IDT core benefit for strong π−π stacking in the solid thin film for enhancement of the efficient charge transport and the conductivity. Meanwhile, the sulfur atoms in IDT are beneficial for passivating the defects at the surface of perovskite, leading to the suppressed recombination of carriers.[21,22] Recently, Chen et al. reported an HTM based on an IDT central core with alkyl side groups bearing two TPA arms for inverted PSCs that attained a PCE of 15.3%.[23] Furthermore, Zhu et al. constructed an HTM featuring an IDT central core with bulky hexylphenyl substituents and two [di(4-methoxyphenyl)amino]carbazole-capped groups, and the planar n-i-p PSCs yielded an impressive PCE of 20.13%.[24] These promising achievements indicated the potential of using the IDT planar core for designing novel dopant-free HTMs. However, IDT-based HTMs are prone to the crystalline phase, resulting in inferior film formation.[23,24] To achieve a highly uniform film in the inverted PSCs, it should avoid crystallization but maintain an amorphous state. To the best of our knowledge, the molecular packing plays a critical role in the film-forming behavior, which is closely related to the hole mobility and crystallization phase of film. Additionally, side-chain engineering of HTMs is an effective strategy to modify the molecular packing, film morphology, charge mobility, and the resultant device performance.[20,25,26] It has been reported that the decent alkyl side chains of HTMs were often critical to solubility in specific solvents and the subsequent molecular

π−π packing behavior in the course of film forming.[27] Another problem regarding the development of the small molecule dopant-free HTMs is the relatively lower fill factor (FF), distributing about 76−81%,[24−26,28] and few dopant-free small molecule HTMs can deliver FF values greater than 81%.[12,40] Considering all the above points, a reasonable way for the promising HTM design is to cut off the symmetrical spirobifluorene core and subsequently insert planar chromophores into the two spiro-linkage fluorenes with twisted units to evolve into orthogonal molecular conformation featuring the extended aromatic coplanar core-linked twisted units. (Scheme 1)

In this work, two rationally designed HTMs based on dibenzofulvene-bridged IDT core attaching hexyl and octyl chains with butterfly-shaped TPA groups have been successfully synthesized, namely, IT-C6 and IT-C8, respectively. Their thermal and optoelectronic properties were tested as HTMs for the fabrication of inverted PSCs. Surprisingly, IT-C8 shows a glass-transition temperature (T_g) of 95 °C, whereas IT-C6 exhibits a marked increase in T_g of 105 °C due to the discrepant molecular packing effect derived from varying alkyl side-chain length.[29] It is revealed that IT-C6 with shorter hexyl chains exhibits a higher hole-transporting mobility, more suitable band energy alignment, and better interfacial contact as well as passivation effect. The champion device of employed HTM based on IT-C6 obtained an 18.34% PCE, which is higher than the longer one with 16.94% PCE. It is noteworthy that both HTM-embodied devices present high fill factors (FF) over 81%, which are among the highest reported values of small molecular HTM-based PSCs (Table S1).

2. RESULTS AND DISCUSSION

The synthetic routes of IT-C6 and IT-C8 can be found in Scheme 2, and the detailed synthetic procedures are shown in the Supporting Information. Our facile synthesis requires only two steps with low complexity. First, IDT-based aldehydes with hexyl and octyl chains as the starting materials were condensed with 2,7-dibromofluorene via the Knoevenagel
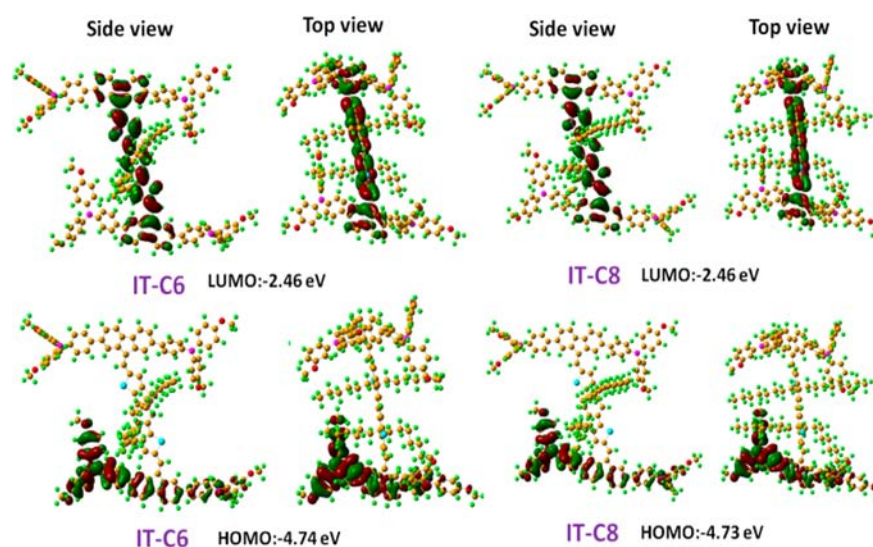
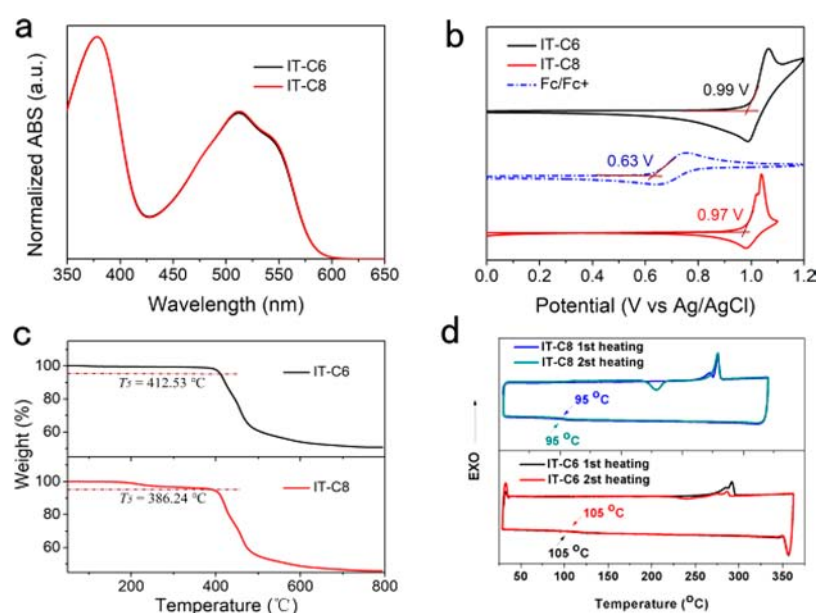**Figure 1.** Density functional calculation of IT-C6 and IT-C8.

Figure 2. (a) UV−vis absorption, (b) CV, (c) TGA, and (d) DSC of IT-C6 and IT-C8.

reaction to yield key intermediates based on dibenzofulvene-bridged Indacenodithiophene core, namely, IT-F-C6 and IT-F-C8, respectively. Subsequently, intermediates IT-F-C6 and IT-F-C8 were coupled with 4-methyloxy-N-(4-methylthiophenyl)-N-(4-(4,4,5,5-tetramethyl-1,3,2-dioxaborolan-2-yl)phenyl)-aniline through a Pd-catalyzed Suzuki coupling to prepare IT-C6 and IT-C8 with isolated yields of 39 and 42%, respectively. The chemical structures of as-prepared compounds were well established by means of ^{1}H nuclear magnetic resonance spectroscopy (NMR), ^{13}C NMR (Figures S1−S8) and matrix-assisted laser desorption ionization time-of-flight (MALDI-TOF) mass spectrometry (Figures S9 and S10). The HTMs (IT-C6 and IT-C8) show good solubility in common organic solvents, such as toluene, chloroform, and chlorobenzene (CB). There is a higher solubility (>15 mg/mL) in CB than that (<3 mg/mL) in DMF and DMSO for the HTMs. Besides, it is observed that the solubility in DMF is little higher than that in DMSO, although the concentration of HTMs is below 3 mg/mL (Figure S11).

Density functional theory (DFT) calculations at the B3LYP/6-31G* level was employed to investigate the highest occupied molecular orbitals (HOMOs) and the lowest unoccupied molecular orbitals (LUMOs) of the IT-C6 and IT-C8 in Figure 1. It is found that the HOMOs are mainly located on the arylamine periphery groups, whereas the LUMOs are mainly localized on dibenzofulvene-bridged indacenodithiophene core of the two molecules. Besides, compared to the spiro-OMeTAD, more extending structures of IT-C6 and IT-C8 were observed via orthogonal arrangement connecting two π-systems, and the torsional angles between the two fluorene attached TPA groups significantly decreased, which is beneficial for obtaining high-quality films.[30] The calculated HOMO energy level for IT-C6 is slightly lower than that of IT-C8, which is consistent with the electrochemical results backward.

The UV−vis absorption curves of films of IT-C6 and IT-C8 were plotted in Figure 2a. Their absorption spectra featuring distinct shoulder absorption peaks are almost coincident,
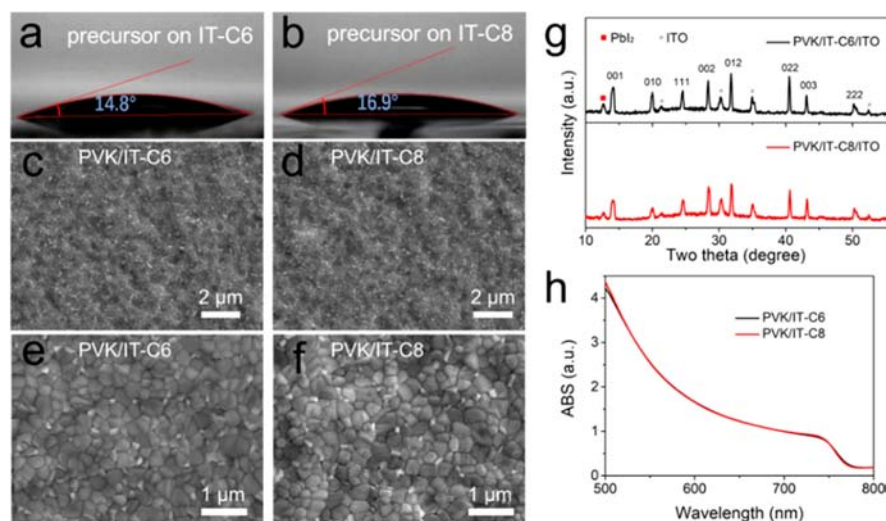
Figure 3. Contact angle of perovskite precursor on (a) IT-C6 film and (b) IT-C8 film, PVK referred to perovskite. The SEM surface morphology of perovskite deposited on (c, e) IT-C6 film and (d, f) IT-C8 film. (g) XRD and (h) UV–vis absorption of perovskite prepared on IT-C6 and IT-C8 substrates.

signifying a typical amorphous-like physical nature.[31] We estimated the optical bandgap (E_g) of IT-C6 and IT-C8 to be ~2.13 eV according to the absorption edge of 580 nm. The HOMOs of both HTMs were measured by means of electrochemical cyclic voltammetry (CV) measurements using ferrocene/ferrocenium (Fc/Fc$^+$) as the internal standard (Figure 2b). According to the formula HOMO = $-[E^{ox} - E(\text{Fc}^+) + 4.8]$ eV, the experimental HOMOs of IT-C6 and IT-C8 are −5.16 and −5.14 eV, respectively, estimated from the oxidation potentials.[8,22] Accordingly, their LUMOs are estimated from the equation LUMO = HOMO + E_g to be −3.03 eV and −3.01 eV for IT-C6 and IT-C8, respectively. Such matched energy levels of IT-C6 and IT-C8 are supposed to be suitable as HTMs for effective hole extraction and electron blocking from perovskite.[26] Thermogravimetric analysis (TGA) and differential scanning calorimetry (DSC) were carried out to investigate the thermal properties of HTMs IT-C6 and IT-C8. As illustrated in Figure 2c, the 5% weight loss temperature (T_5) of IT-C6 and IT-C8 are 412.53 and 386.24 °C, respectively. Both HTMs present excellent thermal stability, which is of vital importance in the realistic device operational conditions.[27] Besides, it was clearly observed that IT-C6 showed a higher thermal decomposition temperature and demonstrated its outstanding thermal stability, which is probably attributed to the shorter hexyl chains inducing the strong self-aggregation of the rigid plane of the backbone. The DSC curves were exhibited in Figure 2d. IT-C8 presents a T_g of 95 °C while IT-C6 exhibits a marked increase in T_g of 105 °C due to the effect of alkyl side-chain length. The hole mobility of two materials were measured according to the space-charge-limited current (SCLC) method (Figure S12) based on the hole-only device with structure of ITO/poly(3,4-ethylenedioxythiophene):polystyrenesulfonate (PEDOT:PSS, 25 nm)/HTMs (25 nm)/MoO$_3$ (8 nm)/Ag.[32] Via Child's law $J_{\text{SCLC}} = 9\varepsilon_0\varepsilon_r\mu V^2/(8L^3)$, in which ε_0 is the permittivity of free space, $\varepsilon_r \approx 3$ is the dielectric constant of the film, μ is the hole mobility, V is the applied voltage and $L \approx 25$ nm are the thicknesses of HTM films, we calculated the hole mobility of IT-C6 and IT-C8 are 9.94×10^{-4} cm^2 V^{-1} s^{-1} and 7.48×10^{-4} cm^2 V^{-1} s^{-1}, respectively, exceeding 1 order of magnitude comparable to the mobility of PTAA (~1×10^{-5} cm^2 V^{-1}

s^{-1}).[33] The fused-ring IDT and fluorene units linked through sp^2-hybridized carbon atom enhance the extended π-conjugation and carrier mobility of both HTMs. The enhanced hole mobility of IT-C6 is probably ascribed from more strengthened molecular packing in the neat film because of the shorter alkyl chains ensuring shorter π–π stacking distance.[27,34]

The contact angle experiments were performed to measure the hydrophilicity of IT-C6 and IT-C8 films with perovskite precursor. Their contact angles are 14.8 and 16.9° for IT-C6 and IT-C8, respectively (Figure 3a, b), reflecting a hydrophilic surface for perovskite solution wetting and completely covering during process, which shows more advantages than the typical hydrophobic hole-transporting polymers including PTAA and PolyTPD.[35] The quality of HTM films and their surface coverage of perovskite crystal are very crucial for interfacial charge transfer that determines the photovoltaic properties of PSCs. Therefore, the surface morphologies of perovskite deposited on IT-C6 and IT-C8 films were explored and recorded in Figure 3c–f. It is hard to evidently distinguish the morphologies of each other from the view of SEM images because of their uniform, dense, and pinhole-free perovskite films, which is significant to avoid short circuit occurring. Some excessive PbI$_2$ at the grain boundary was observed, which is also confirmed by X-ray diffraction (XRD) (Figure 3g). It should be pointed out that the residual PbI$_2$ is beneficial to passivate the defects of grain boundaries in perovskite films.[36] A zoomed-in surface morphology of perovskite deposited on different substrates was also measured by atomic force microscopy (AFM) as shown in Figure S13. The root-mean-square values (RMS) of perovskite on IT-C6 (14.03 nm) are nearly consistent with that on quartz (13.56 nm), whereas the RMS on IT-C8 (20.38 nm) reveals a relatively rough surface morphology indicating the formation of a smoother film of IT-C6 due to the employed shorter side chains and the subtle difference of substrate hydrophilicity. This may render an effective interfacial contact between the perovskite/HTM or the HTM/anode, leading to an optimized FF of PSCs.[34] AFM was further conducted to investigate the film morphology before and after being rinsed by perovskite precursor solvents DMF/DMSO (v/v 4/1). As exhibited in Figure S14, before
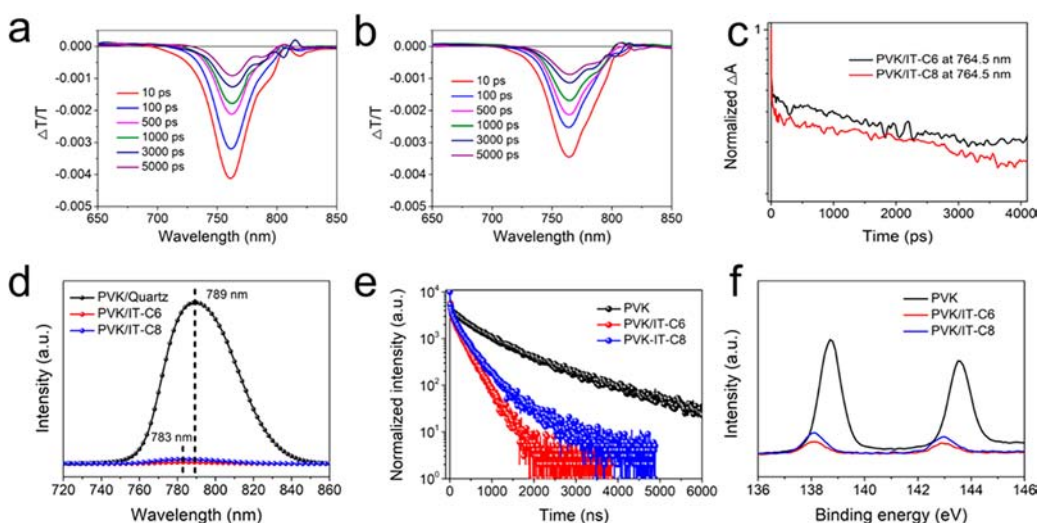
Figure 4. Transient absorption of perovskite on (a) IT-C6 and (b) IT-C8 substrates at different time delays after laser excitation at 630 nm. (c) Normalized time-resolved absorption density of perovskite films excited probed at 764.5 nm. (d) PL and (e) TRPL and (f) XPS of perovskite contacted with quartz, IT-C6, and IT-C8.

being rinsed, IT-C6 and IT-C8 on ITO substrate present root-mean-square (RMS) values of 2.15 and 3.17 nm, respectively. After rinsed, the RMS values increase to 7.11 nm for IT-C6 film and 7.18 nm for IT-C8 film. It indicates that the smooth film morphology is possibly influenced during perovskite deposition because of the dissolution of a small amount of HTMs by precursor solvents. However, the HTMs remain whole layer between ITO and perovskite due to very short processing time. During the measurement of surface roughness, scanning Kelvin probe microscopy (SKPM) was performed to obtain the surface potential mappings simultaneously. The surface potential of HTMs contacted perovskite films is negative, whereas the quartz contacted perovskite film is positive. The decreased surface potential is related to the bottom selective contact, and more negative probed surface reflects a higher charge transfer efficiency resulting from the hole extraction of HTMs IT-C6, IT-C8.[37] The UV−vis absorption (Figure 3 h) of both films shows ignorable discrepancy, and the E_g values of perovskite films were estimated to be 1.59 eV, which is consistent with the reported bandgap of the same perovskite composition.[38]

Transient absorption spectroscopy (TAS), photoluminescence (PL) and time-resolved photoluminescence (TRPL) were further conducted to study the charge transfer dynamics of HTMs. The TAS profiles were depicted in Figure 4a−c. Perovskite on IT-C6 (Figure 4a) exhibited a stronger photon bleaching than that on IT-C8 (Figure 4b). Besides, in the normalized TAS time profiles (Figure 4c), the IT-C6 treated film also displays a longer-lived signal within nanosecond times probed at the wavelength of 764.5 nm, hinting at a greater charge-pair separation and suppressed nonradiative recombination.[39] In the steady-state PL, perovskite films deposited on quartz, IT-C6, and IT-C8 were excited with an incident light at a wavelength of 550 nm as shown in Figure 4d. A bright PL peak of PVK/quartz was observed and suddenly quenched once IT-C6 and IT-C8 were inserted because of the rapid hole transfer. A greater intensity reduction caused by IT-C6 instead of IT-C8 indicates a faster hole extraction rate from the perovskite to HTM. It was obviously observed that the PL intensity of the PVK/IT-C6 is weaker than the PVK/IT-C8 because of the shorter alkyl chain, indicating a faster hole

extraction rate from the perovskite to IT-C6 in Figure S15. The TRPL (Figure 4e) spectra of perovskite with or without HTMs also agreed well with foregoing results. We fitted the decay lifetime curves using the double-exponential formula $I(t) = A_1 \exp(-t/\tau_1) + A_2 \exp(-t/\tau_2)$, and their fitting parameters A_1, A_2, τ_1, τ_2, and τ_{av} ($\tau_{av} = A_1\tau_1 + A_2\tau_2$) are listed in Table S2. The average lifetime τ_{av} are 243.09, 354.12, and 1107.30 ns for PVK/IT-C6, PVK/IT-C8, and PVK/quartz, respectively. This indicates that the PL lifetime of perovskite showing relatively inferior hole extraction decreases obviously when IT-C6 and IT-C8 were used as HTMs, and the perovskite/IT-C6 interface shows faster hole collection relative to the perovskite/IT-C6 interface. The accelerated hole extraction may originate from the enhanced molecular packing of IT-C6 to form a denser pinhole-free film due to an improved interfacial contact. From the enlarged PL spectra (Figure S15), we noticed that the PL peaks of PVK/HTLs shift to 783 nm compared to the pristine perovskite located at 789 nm. The 6 nm blue shift of HTM contacted perovskite film may be on account of the passivation of defects via Lewis acid−base interaction between S and Pb.[40] Previous work[41−44] based on interface passivation did not show PL peak shift due to the almost unchanged bandgap of bulk perovskite itself. However, in our study, a small amount of HTMs were inevitably dissolved by precursor during the formation of perovskite film, which may influence the bandgap of perovskite itself. Thus, the PL blue shift of PVK/HTLs compared to the pristine perovskite possibly comes from the traps' removal of perovskite grain boundaries, which narrows the bandgap of bulk perovskite. To demonstrate the passivation effect of HTMs on perovskite, we carried out X-ray photoelectron spectroscopy (XPS) to measure the Pb peaks, as shown in Figure 4f. The Pb peaks of HTMs covered the perovskite shift of approximately 0.7 eV toward the low binding energy direction from pristine perovskite, evidently validating the passivation effect of IT-C6 and IT-C8 on perovskite.[45]

To evaluate the photovoltaic performance of IT-C6 and IT-C8 as dopant-free HTM in PSCs, we fabricated inverted perovskite solar cells with a device architecture of ITO/HTM/perovskite/$PC_{61}BM$/ZrAcac/Ag. The device structure diagram and its SEM cross-section image are shown in Figure 5a and
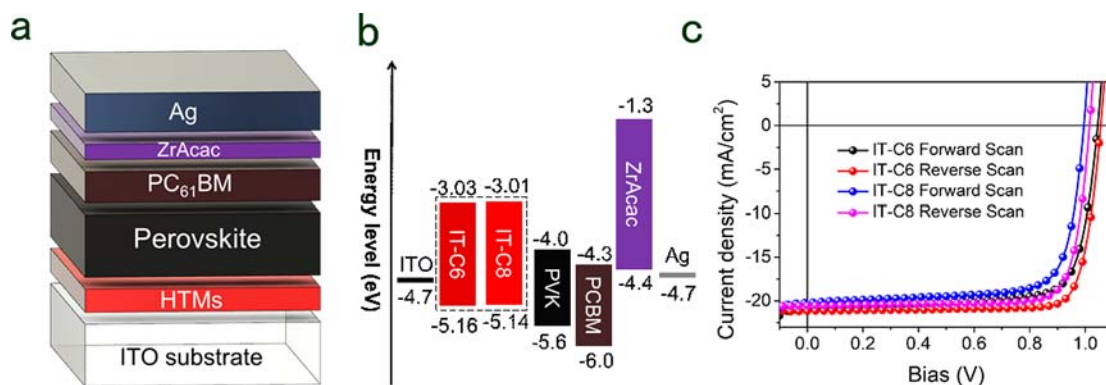
Figure 5. (a) Device structure diagram, (b) band energy alignment, and (c) $J-V$ curves of the champion devices. IT-C6 was annealed at 160 °C and IT-C6 was annealed at 120 °C.

Figure S16, respectively. The band energy alignment was shown in Figure 5b, where the HOMO and LUMO values of HTMs were obtained from above CV and UV−vis absorption and others were taken from the literature.[46,47] To study the dependence of device performance on the solution concentration of HTMs, we dissolved IT-C6 and IT-C8 in CB with linearly increasing concentrations of 2, 3, 4, 5, and 7 mg/mL. The changing performance parameters based on the corresponding devices with different concentrations of HTMs such as open-circuit voltage (V_{oc}), short-circuit current density (J_{sc}), FF, and power conversion efficiency (PCE) are plotted in Figure S17. With the increase in HTM concentration, all these parameters present certain trends, where their V_{oc} values creep up while FF creeps down and J_{sc} and PCE show a trend of increasing first and then decreasing. Surprisingly, our results reveal that the FF of IT-C6 and IT-C8 HTMs are greater than 80% at low concentrations (2 or 3 mg/mL), and the highest values of IT-C6 and IT-C8 HTMs are 86.35% (at 2 mg/mL) and 81.71% (at 2 mg/mL), respectively. The optimal concentration for the highest average PCE for IT-C6 and IT-C8 is 3 mg/mL, as listed in Table S3. After optimization of the annealing temperature of IT-C6 (160 °C) and IT-C8 (120 °C), we achieved the IT-C6- and IT-C8-based champion devices whose $J-V$ curves are depicted in Figure 5c and their photovoltaic performance parameters are listed in Table 1. IT-C6 champion device has a reverse scanned PCE of

Table 1. Photovoltaic Performance Parameters of IT-C6 & IT-C8-Based Champion Devices

HTMs	scan direction	V_{oc} (V)	J_{sc} (mA/cm^2)	FF (%)	PCE (%)	Int.J_{sc} (mA/cm^2)
IT-C6	forward scan	1.045	20.86	76.48	16.67	20.95
	reverse scan	1.055	21.17	82.32	18.34	
IT-C8	forward scan	0.995	20.21	75.72	15.23	20.27
	reverse scan	1.016	20.54	81.20	16.94	

18.34% (V_{oc} = 1.055 V, J_{sc} = 21.17 mA/cm^2, FF = 82.32%), whereas the PCE of IT-C8 device is 16.94% (V_{oc} = 1.016 V, J_{sc} = 20.54 mA/cm^2, FF = 81.20%). It is obvious that the PSCs based on IT-C6 HTM have significantly enhanced conversion efficiencies relative to the IT-C8 based device due to the simultaneous improvements in J_{sc} and FF, which are possibly

attributed to the denser pinhole-free film, higher hole transport, and suitable interfacial contact layer.[20,36]

Their external quantum efficiencies (EQE) are shown in Figure 6a. From the EQE curves, we obtained integrated J_{sc} values of 20.95 and 20.27 mA/cm^2 for IT-C6 and IT-C8 champion devices, respectively, which is in good agreement with the $J-V$ measurements. The two devices exhibit close J_{sc} and FF but an obvious difference in V_{oc}, which is highly related with the nonradiative recombination process of operational devices.[48] To analyze their V_{oc} disparity, we measured the device dark current and electrochemical impedance spectroscopy (EIS). Figure 6b presents that the leakage current (J_0) is reduced from 4.21 × 10^{-3} mA/cm^2 to 1.48 × 10^{-3} mA/cm^2, which signifies increased V_{oc} in terms of the equation $V_{oc} = kT/q\ln(J_{sc}/J_0 + 1)$, where V_{oc} is the open circuit voltage, q the elementary charge, k the Boltzmann constant, T the absolute temperature, J_{sc} the short circuit current, and J_0 the dark current leakage.[46,48] The Nyquist plots (Figure 6c) of EIS fitting by the inset equivalent circuit were exhibited to investigate the charge carrier transport in the devices. The larger semicircular shape indicating a higher recombination resistance (R_{REC}), which explains the higher V_{oc} of the IT-C6 device originating from the suppressed nonradiative recombination losses.[49,50] We assumed the decreased recombination was attributable to the passivation extent of HTMs on the perovskite layer. Thus, we fabricated hole-only devices with structure of ITO/HTMs/perovskite/spiro-OMeTAD/Au to compare their trap state density following the relation $N_t = 2\varepsilon_0\varepsilon_r V_t/eL$, where ε_0 is the vacuum permittivity, ε_r the relative permittivity of perovskite, e the charge constant, and L the film thickness of perovskite.[51] The trap-filled limited voltage (V_t) can be read from the intersection of linear fits of Ohmic regime and SCLC regime in the $J-V$ curves of hole-only devices as shown in Figure 6d.[52] The IT-C6 hole-only device with a smaller V_t = 0.07 V than V_t = 0.27 V of IT-C8 device proves the decreased trap-state density from 1.57 × 10^{15} cm^{-3} to 4.08 × 10^{14} cm^{-3}. The improved passivation effect of IT-C6 is probably on account of the better interfacial contact due to the weaker steric hindrance of shorter alkyl chain between HTM and perovskite. The V_{oc} and J_{sc} changes with a function of light intensity were measured to study the charge recombination process along the entire solar cells.[1] The IT-C6 device ideal factor n = 1.173 is lower than n = 1.423 of IT-C8 device (Figure 6e), indicating an inhibited trap-assisted nonradiative recombination loss. J_{sc} with the change of light intensity presents a linear correlation (slope = 1) for both devices
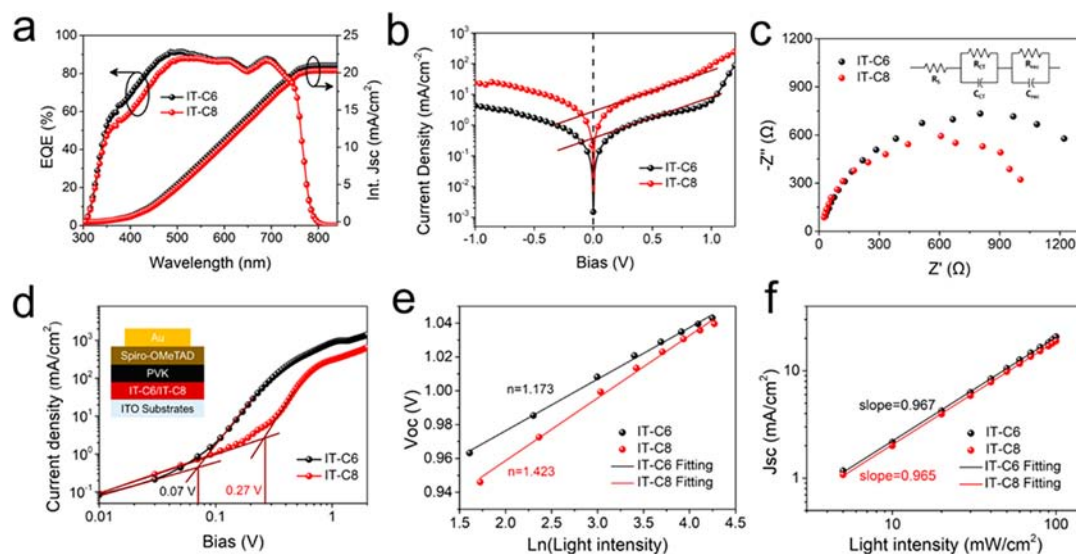
Figure 6. (a) EQE and integrated J_{sc}, (b) dark current curves, (c) EIS Nyquist plot, (d) $J-V$ curves of hole-only devices, (e) V_{oc}, and (f) J_{sc} of perovskite solar cells as a function of light intensity.
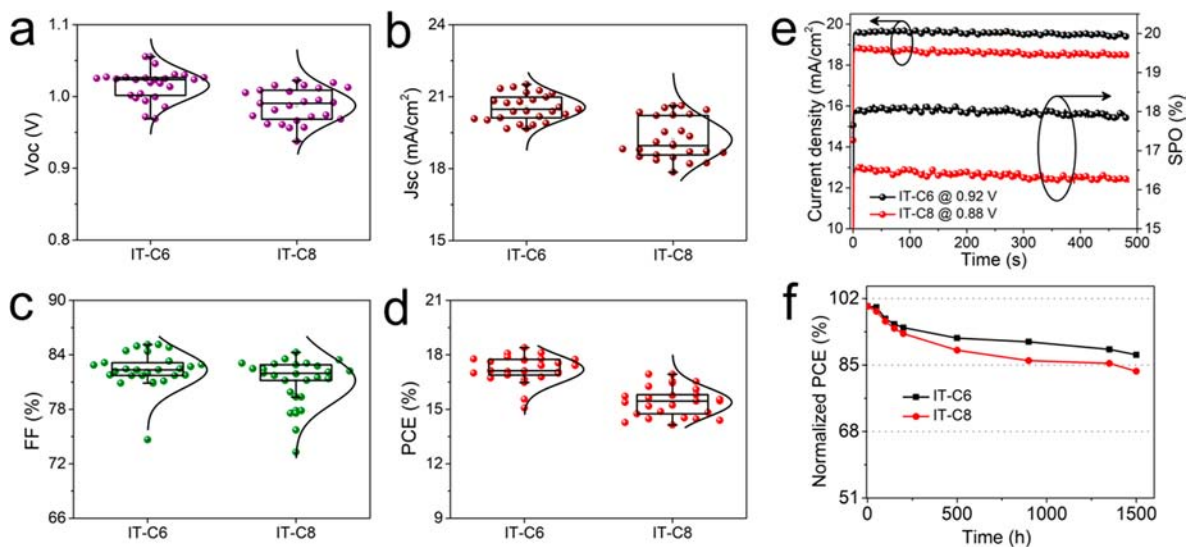

Figure 7. Statistics of photovoltaic parameters (a) V_{oc}, (b) J_{sc}, (c) FF, and (d) PCE based on 25 devices. (e) Stabilized power-out and (f) stability of perovskite solar cells measured in a glovebox.

(Figure 6f), reflecting almost no radiative recombination in the operational condition. Overall, IT-C6 with a shorter alkyl chain length behaves better in defect passivation and inhibits nonradiative recombination on the perovskite layer as also manifested by TAS, PL, TRPL, and XPS measurements, which enables higher V_{oc}, J_{sc}, FF, and PCE for photovoltaic devices.

The statistics of performance parameters (V_{oc}, J_{sc}, FF, and PCE) of reverse-scan-measured IT-C6 and IT-C8 devices fabricated under optimized circumstances are shown in Figure 7a−d. IT-C6 devices harvest an average V_{oc} 1.015 ± 0.020, J_{sc} 20.56 ± 0.54, FF 82.35 ± 1.98, and PCE 17.20 ± 0.74, whereas IT-C8 devices have a decreased average V_{oc} 0.987 ± 0.023, J_{sc} 19.20 ± 0.83, FF 81.19 ± 2.56, and PCE 15.39 ± 0.78. The reliable performance statistics of both devices gave a conclusion that the shorter alkyl chain length HTM IT-C6 verifies more reproducibly excellent device light-to-electrical energy conversion efficiency than IT-C8. For the safe of accuracy, we also confirmed the device PCE by measuring the

stabilized current density output at the maximum power point as shown in Figure 7e. The stabilized power output (SPO) of the IT-C6 device is about ∼18.0% under 0.92 V bias, whereas the IT-C8 device is about ∼16.2% under 0.88 V bias. Their stable operation measured within 8 min proved good illumination stability as well, which benefited from the mixed organic−inorganic perovskite composition. The stability of unsealing devices was measured in glovebox under dark conditions in varying hours. As depicted in Figure 7f, the PCEs of both devices drop rather tardily and maintain above 85% efficiency of the initial value within 1350 h; however, the IT-C8 involved device exhibits a relatively rapid decline. We also measured the device stability in air with high humidity (50−75%) and in high temperature (65 °C) conditions, as shown in Figures S18 and S19. The performance of unencapsulated devices measured in air with high humidity (50−75%) presents fast dropping within 1 week. For the stability measured in high-temperature (65 °C) conditions, a more rapid decrease to 85%

of their initial PCE was obtained. The fast reduction of device performance when measured out of the glovebox in thermal conditions may result from the metal electrode oxidation and perovskite degradation induced by oxygen and humidity penetration as well as thermal stimulus. The better stability of the IT-C6 device is probably due to its more advantageous interfacial contact and passivation effect, leading to decreased trap-state density that is a common factor to induce degradation of perovskite films.[53,54]

3. CONCLUSION

In summary, two novel hole HTMs (IT-C6 and IT-C8) based on dibenzofulvene-bridged IDT core attaching hexyl and octyl chains with butterfly-shaped TPA groups are designed and synthesized for inverted PSCs. It is revealed that the IT-C6 with hexyl chain exhibits obviously enhanced T_g, higher hole-transporting mobility, more suitable band energy alignment, better interfacial contact as well as passivation effect in respect to IT-C8 with octyl chain. Furthermore, the champion device of employed HTM based on IT-C6 achieved a PCE of 18.34% with a high FF of 82.32% in comparison to 16.94% PCE of IT-C8-based device with a high FF of 81.20%, which are among the highest reported values of small molecular HTMs based PSCs. Our study reveals that the combination of IDT with varying alkyl chains and spiro-linkage fluorine with twisted units via tailoring rationally the spiro-core is an effective strategy to design promising HTMs for the inverted PSCs.

■ ASSOCIATED CONTENT

ⓢ Supporting Information

The Supporting Information is available free of charge at https://pubs.acs.org/doi/10.1021/acsami.0c22993.

> Synthesis of hole-transporting materials, property tests of hole-transporting materials, film characterizations, and device measurements (PDF)

■ AUTHOR INFORMATION

Corresponding Authors

Guangbo Che — *Key Laboratory of Preparation and Application of Environmental-Friendly Materials, Jilin Normal University, Ministry of Education, Changchun 130103, P.R. China;* ⓞ orcid.org/0000-0001-8884-8150; Email: guangboche@jlnu.edu.cn

Hsing-lin Wang — *Department of Materials Science and Engineering, Southern University of Science and Technology, Shenzhen 518055, P.R. China;* ⓞ orcid.org/0000-0002-6379-0519; Email: wangxl3@sustech.edu.cn

Authors

Enwei Zhu — *Key Laboratory of Preparation and Application of Environmental-Friendly Materials, Jilin Normal University, Ministry of Education, Changchun 130103, P.R. China*

Jiantao Wang — *Department of Materials Science and Engineering, Southern University of Science and Technology, Shenzhen 518055, P.R. China; Department of Chemistry, Hong Kong University of Science and Technology, Hong Kong S.A.D., P.R. China;* ⓞ orcid.org/0000-0002-1929-3339

Jing Xu — *Department of Materials Science and Engineering, Southern University of Science and Technology, Shenzhen 518055, P.R. China*

Liying Fu — *Key Laboratory of Preparation and Application of Environmental-Friendly Materials, Jilin Normal University, Ministry of Education, Changchun 130103, P.R. China*

Ruxue Li — *Department of Electrical and Electronic Engineering, Southern University of Science and Technology, Shenzhen 518055, P.R. China*

Chengzhuo Yu — *Department of Materials Science and Engineering, Southern University of Science and Technology, Shenzhen 518055, P.R. China*

Shijie Ge — *Department of Materials Science and Engineering, Southern University of Science and Technology, Shenzhen 518055, P.R. China*

Xiaosong Lin — *Department of Materials Science and Engineering, Southern University of Science and Technology, Shenzhen 518055, P.R. China*

Rui Chen — *Department of Electrical and Electronic Engineering, Southern University of Science and Technology, Shenzhen 518055, P.R. China;* ⓞ orcid.org/0000-0002-0445-7847

Hongkai Wu — *Department of Chemistry, Hong Kong University of Science and Technology, Hong Kong S.A.D., P.R. China;* ⓞ orcid.org/0000-0002-7766-7888

Complete contact information is available at:
https://pubs.acs.org/10.1021/acsami.0c22993

Author Contributions

[†]E.Z. and J.W. contributed equally to this work.

Notes

The authors declare no competing financial interest.

■ ACKNOWLEDGMENTS

■ REFERENCES

(1) Yang, W.; Park, B. W.; Jung, E. H.; Jeon, N. J.; Kim, Y. C.; Lee, D. U.; Shin, S. S.; Seo, J.; Kim, E. K.; Noh, J. H.; Seok, S. I. Iodide Management in Formamidinium-Lead-Halide-Based Perovskite Layers for Efficient Solar Cells. *Science* **2017**, *356*, 1376−1379.

(2) Jiang, Q.; Zhao, Y.; Zhang, X.; Yang, X.; Chen, Y.; Chu, Z.; Ye, Q.; Li, X.; Yin, Z.; You, J. Surface Passivation of Perovskite Film for Efficient Solar Cells. *Nat. Photonics* **2019**, *13*, 460−466.

(3) NREL. *Best Research-Cell Efficiency Chart.* https://www.nrel.gov/pv/assets/pdfs/cell-pv-eff-emergingpv.202001042.pdf.

(4) Li, F.; Deng, X.; Qi, F.; Li, Z.; Liu, D.; Shen, D.; Qin, M.; Wu, S.; Lin, F.; Jang, S.; et al. Regulating Surface Termination for Efficient Inverted Perovskite Solar Cells with Greater Than 23% Efficiency. *J. Am. Chem. Soc.* **2020**, *142*, 20134−20142.

(5) Zheng, X.; Hou, Y.; Bao, C.; Yin, J.; Yuan, F.; Huang, Z.; Song, K.; Liu, J.; Troughton, J.; Gasparini, N.; et al. Managing Grains and Interfaces Via Ligand Anchoring Enables 22.3%-Efficiency Inverted Perovskite Solar Cells. *Nat. Energy.* **2020**, *5*, 131−140.

(6) Al-Ashouri, A.; Kohnen, E.; Li, B.; Magomedov, A.; Hempel, H.; Caprioglio, P.; Marquez, J. A.; Morales Vilches, A. B.; Kasparavicius,

E.; Smith, J. A.; et al. Monolithic Perovskite/silicon Tandem Solar Cell with > 29% Efficiency by Enhanced Hole Extraction. *Science* **2020**, *370*, 1300−1309.

(7) Jeong, M.; Choi, W.; Go, E. M.; Cho, Y.; Kim, M.; Lee, B.; Jeong, S.; Jo, Y.; Choi, H. W.; Lee, J.; Bae, J. H.; Kwak, S. K.; Kim, D. S.; Yang, C. Stable Perovskite Solar Cells with Efficiency Exceeding 24.8% and 0.3V Voltage Loss. *Science* **2020**, *369*, 1615−1620.

(8) Zhou, J.; Yin, X.; Dong, Z.; Ali, A.; Song, Z.; Shrestha, N.; Bista, S. S.; Bao, Q.; Ellingson, R. J.; Yan, Y.; Tang, W. Dithieno [3,2-b:2′, 3′-d] pyrrole Cored p-Type Semiconductors Enabling 20% Efficiency Dopant-Free Perovskite Solar Cells. *Angew. Chem., Int. Ed.* **2019**, *58*, 13717−13721.

(9) Bi, D.; Tress, W.; Dar, M. I.; Gao, P.; Luo, J.; Renevier, C.; Schenk, K.; Abate, A.; Giordano, F.; Baena, J. C.; Decoppet, J. D.; Zakeeruddin, S. M.; Nazeeruddin, M. K.; Grätzel, M.; Hagfeldt, A. Efficient Luminescent Solar Cells Based on Tailored Mixed-cation Perovskites. *Sci. Adv.* **2016**, *2*, e1501170.

(10) Xu, B.; Bi, D.; Hua, Y.; Liu, P.; Cheng, M.; Graetzel, M.; Kloo, L.; Hagfeldt, A.; Sun, L. A Low-Cost Spiro[fluorene-9,9′-xanthene]-Based Hole Transport Material for Highly Efficient Solid-state Dye-sensitized Solar Cells and Perovskite Solar Cells. *Energy Environ. Sci.* **2016**, *9*, 873−877.

(11) Zhang, J.; Xu, B.; Yang, L.; Ruan, C.; Wang, L.; Liu, P.; Zhang, W.; Vlachopoulos, N.; Kloo, L.; Boschloo, G.; Sun, L.; Hagfeldt, A.; Johansson, E. M. J. The Importance of Pendant Groups on Triphenylamine-Based Hole Transport Materials for Obtaining Perovskite Solar Cells with over 20% Efficiency. *Adv. Energy Mater.* **2018**, *8*, 1701209.

(12) Wang, Y.; Chen, W.; Wang, L.; Tu, B.; Chen, T.; Liu, B.; Yang, K.; Koh, C. W.; Zhang, X.; Sun, H.; et al. Dopant-Free Small-Molecule Hole-Transporting Material for Inverted Perovskite Solar Cells with Efficiency Exceeding 21%. *Adv. Mater.* **2019**, *31*, 1902781.

(13) Wang, J.; Zhang, H.; Wu, B.; Wang, Z.; Sun, Z.; Xue, S.; Wu, Y.; Hagfeldt, A.; Liang, M. Indeno[1,2-b]carbazole as Methoxy-Free Donor Group: Constructing Efficient and Stable Hole-Transporting Materials for Perovskite Solar Cells. *Angew. Chem., Int. Ed.* **2019**, *58*, 15721−15725.

(14) Seo, J.; Kim, H.; Akin, S.; Stojanovic, M.; Simon, E.; Fleischer, M.; Hagfeldt, A.; Zakeeruddin, S. M.; Grätzel, M. Novel p-dopant Toward Highly Efficient and Stable Perovskite Solar Cells. *Energy Environ. Sci.* **2018**, *11*, 2985−2992.

(15) Wang, C.; Xiao, C.; Yu, Y.; Zhao, D.; Awni, R. A.; Grice, C. R.; Ghimire, K.; Constantinou, D.; Liao, W.; Cimaroli, A. J.; Liu, P.; Chen, J.; Podraza, N. J.; Jiang, C.; Al-Jassim, M. M.; Zhao, X.; Yan, Y. Understanding and Eliminating Hysteresis for Highly Efficient Planar Perovskite Solar Cells. *Adv. Energy Mater.* **2017**, *7*, 1700414.

(16) Urieta-Mora, J.; García-Benito, I.; Molina-Ontoria, A.; Martín, N. Hole Transporting Materials for Perovskite Solar Cells: a Chemical Approach. *Chem. Soc. Rev.* **2018**, *47*, 8541−8571.

(17) Zhou, W.; Wen, Z.; Gao, P. Less is More: Dopant-Free Hole Transporting Materials for High-Efficiency Perovskite Solar Cells. *Adv. Energy Mater.* **2018**, *8*, 1702512.

(18) Lin, Y.; Wang, J.; Zhang, Z.; Bai, H.; Li, Y.; Zhu, D.; Zhan, X. An Electron Acceptor Challenging Fullerenes for Efficient Polymer Solar Cells. *Adv. Mater.* **2015**, *27*, 1170−1174.

(19) Lin, Y.; He, Q.; Zhao, F.; Huo, L.; Mai, J.; Lu, X.; Su, C.; Li, T.; Wang, J.; Zhu, J.; Sun, Y.; Wang, C.; Zhan, X. A Facile Planar Fused-Ring Electron Acceptor for As-Cast Polymer Solar Cells with 8.71% Efficiency. *J. Am. J. Am. Chem. Soc.* **2016**, *138*, 2973−2976.

(20) Li, Y.; Zheng, N.; Yu, L.; Wen, S.; Gao, C.; Sun, M.; Yang, R. A Simple Phenyl Group Introduced at the Tail of Alkyl Side Chains of Small Molecular Acceptors: New Strategy to Balance the Crystallinity of Acceptors and Miscibility of Bulk Heterojunction Enabling Highly Efficient Organic Solar Cells. *Adv. Mater.* **2019**, *31*, 1807832.

(21) Chen, H.; Fu, W.; Huang, C.; Zhang, Z.; Li, S.; Ding, F.; Shi, M.; Li, C.; Jen, A. K.-Y.; Chen, H. Molecular Engineered Hole-Extraction Materials to Enable Dopant-Free, Efficient p-i-n Perovskite Solar Cells. *Adv. Energy Mater.* **2017**, *7*, 1700012.

(22) Meng, F.; Jia, Y.; Wang, J.; Huang, X.; Gui, Z.; Huang, L.; Li, R.; Chen, R.; Xu, J.; Chen, W.; He, Z.; Hsu, H. Y.; Zhu, E.; Che, G.; Wang, H. L. Dopant-Free Hole Transporting Molecules for Highly Efficient Perovskite Photovoltaic with Strong Interfacial Interaction. *Sol. RRL.* **2019**, *3*, 1900319.

(23) Liu, X.; Rezaee, E.; Shan, H.; Xu, J.; Zhang, Y.; Feng, Y.; Dai, J.; Chen, Z. K.; Huang, W.; Xu, Z. X. Dopant-free Hole Transport Materials Based on Alkyl-substituted Indacenodithiophene for Planar Perovskite Solar Cells. *J. Mater. Chem. C* **2018**, *6*, 4706−4713.

(24) Hua, Y.; Chen, S.; Zhang, D.; Xu, P.; Sun, A.; Ou, Y.; Wu, T.; Sun, H.; Cui, B.; Zhu, X. Bis[di(4-methoxyphenyl)amino]carbazole-capped Indacenodithiophenes As Hole Transport Materials for Highly Efficient Perovskite Solar Cells: the Pronounced Positioning Effect of a Donor Group on the Cell Performance. *J. Mater. Chem. A* **2019**, *7*, 10200−10205.

(25) Shen, C.; Wu, Y.; Zhang, H.; Li, E.; Zhang, W.; Xu, X.; Wu, W.; Tian, H.; Zhu, W. H. Semi-Locked Tetrathienylethene as a Building Block for Hole-Transporting Materials: Toward Efficient and Stable Perovskite Solar Cells. *Angew. Chem., Int. Ed.* **2019**, *58*, 3784−3789.

(26) Lai, X.; Du, M.; Meng, F.; Li, G.; Li, W.; Kyaw, A. K. K.; Wen, Y.; Liu, C.; Ma, H.; Zhang, R.; Fan, D.; Guo, X.; Wang, Y.; Ji, H.; Wang, K.; Sun, X.; Wang, J.; Huang, W. High-Performance Inverted Planar Perovskite Solar Cells Enhanced by Thickness Tuning of New Dopant-Free Hole Transporting Layer. *Small* **2019**, *15*, 1904715.

(27) Tu, B.; Wang, Y.; Chen, W.; Liu, B.; Feng, X.; Zhu, Y.; Yang, K.; Zhang, Z.; Shi, Y.; Guo, X.; Li, H.; Tang, Z.; Djurisic, A. B.; He, Z. Side-Chain Engineering of Donor-Acceptor Conjugated Small Molecules as Dopant-Free Hole-Transport Materials for Efficient Normal Planar Perovskite Solar Cells. *ACS Appl. Mater. Interfaces* **2019**, *11*, 48556−48563.

(28) Rakstys, K.; Paek, S.; Gao, P.; Gratia, P.; Marszalek, T.; Grancini, G.; Cho, K. T.; Genevicius, K.; Jankauskas, V.; Pisula, W.; Nazeeruddin, M. K. Molecular Engineering of Face-on Oriented Dopant-free Hole Transporting Material for 19% Perovskite Solar Cells. *J. Mater. Chem. A* **2017**, *5*, 7811−7815.

(29) Wang, J.; Zhang, H.; Wu, B.; Wang, Z.; Sun, Z.; Xue, S.; Wu, Y.; Hagfeldt, A.; Liang, M. Indeno[1,2-b]carbazole as Methoxy-Free Donor Group: Constructing Efficient and Stable Hole-Transporting Materials for Perovskite Solar Cells. *Angew. Chem., Int. Ed.* **2019**, *58*, 15721−15725.

(30) Wang, X.; Zhang, J.; Yu, S.; Yu, W.; Fu, P.; Liu, X.; Tu, D.; Guo, X.; Li, C. Lowering Molecular Symmetry to Improve the Morphological Properties of the Hole-Transport Layer for Stable Perovskite Solar Cells. *Angew. Chem., Int. Ed.* **2018**, *57*, 12529−12533.

(31) Park, S. J.; Jeon, S.; Lee, I. K.; Zhang, J.; Jeong, H.; Park, J. Y.; Bang, J.; Ahn, T. K.; Shin, H. W.; Kim, B. G.; Park, H. J. Inverted Planar Perovskite Solar Cells with Dopant Free Hole Transporting Material: Lewis base-assisted Passivation and Reduced Charge Recombination. *J. Mater. Chem. A* **2017**, *5*, 13220−13227.

(32) Snaith, H. J.; Grätzel, M. Enhanced Charge Mobility in a Molecular Hole Transporter Via Addition of Redox Inactive ionic Dopant: Implication to Dye-sensitized Solar Cells. *Appl. Phys. Lett.* **2006**, *89*, 262114.

(33) Huang, C.; Fu, W.; Li, C. Z.; Zhang, Z.; Qiu, W.; Shi, M.; Heremans, P.; Jen, A. K. Y.; Chen, H. Dopant-Free Hole-Transporting Material with a C3h Symmetrical Truxene Core for Highly Efficient Perovskite Solar Cells. *J. Am. Chem. Soc.* **2016**, *138*, 2528−2531.

(34) Kwon, H.; Reddy, S. S.; Arivunithi, V. M.; Jin, H.; Park, H. Y.; Cho, W.; Song, M.; Jin, S. H. A linear D-π-A Based Hole Transport Material for High Performance Rigid and Flexible Planar Organic-inorganic Hybrid Perovskite Solar Cells. *J. Mater. Chem. C* **2019**, *7*, 13440−13446.

(35) Liu, X.; Cheng, Y.; Liu, C.; Zhang, T.; Zhang, N.; Zhang, S.; Chen, J.; Xu, Q.; Ouyang, J.; Gong, H. Correction: 20.7% Highly Reproducible Inverted Planar Perovskite Solar Cells with Enhanced Fill Factor and Eliminated Hysteresis. *Energy Environ. Sci.* **2019**, *12*, 1718−1718.

(36) Wang, J.; Meng, F.; Li, R.; Chen, S.; Huang, X.; Xu, J.; Lin, X.; Chen, R.; Wu, H.; Wang, H. Boosting Efficiency and Stability of Planar Inverted $(FAPbI_3)_x(MAPbBr_3)_{1-x}$ Solar Cells via $FAPbI_3$ and $MAPbBr_3$ Crystal Powders. *Sol. RRL* **2020**, *4*, 2000091.

(37) Wu, Y.; Chen, W.; Lin, Y.; Tu, B.; Lan, X.; Wu, Z.; Liu, R.; Djurišić, A.; He, Z. General Method To Define the Type of Carrier Transport Materials for Perovskite Solar Cells Via Kelvin Probes Microscopy. *ACS Appl. Energy Mater.* **2018**, *1*, 3984−3991.

(38) Wu, S.; Zhang, J.; Li, Z.; Liu, D.; Qin, M.; Cheung, S.; Lu, X.; Lei, D.; So, S.; Zhu, Z.; Jen, A. Modulation of Defects and Interfaces through Alkylammonium Interlayer for Efficient Inverted Perovskite Solar Cells. *Joule.* **2020**, *4*, 1248−1262.

(39) Chen, W.; Wang, Y.; Pang, G.; Koh, C.; Djurišić, A.; Wu, Y.; Tu, B.; Liu, F.; Chen, R.; Woo, H.; Guo, X.; He, Z. Conjugated Polymer-Assisted Grain Boundary Passivation for Efficient Inverted Planar Perovskite Solar Cells. *Adv. Funct. Mater.* **2019**, *29*, 1808855.

(40) Zhang, J.; Sun, Q.; Chen, Q.; Wang, Y.; Zhou, Y.; Song, B.; Jia, X.; Zhu, Y.; Zhang, S.; Yuan, N.; Ding, J.; Li, Y. Dibenzo[b,d]-thiophene-Cored Hole-Transport Material with Passivation Effect Enabling the High-Efficiency Planar p-i-n Perovskite Solar Cells with 83% Fill Factor. *Sol. RRL.* **2020**, *4*, 1900421.

(41) Yang, S.; Chen, S.; Mosconi, E.; Fang, Y.; Xiao, X.; Wang, C.; Zhou, Y.; Yu, Z.; Zhao, J.; Gao, Y.; et al. Stabilizing Halide Perovskite Surfaces for Solar Cell Operation with Wide-Bandgap Lead Oxysalts. *Science* **2019**, *365*, 473−478.

(42) Zhou, Y.; Wang, F.; Cao, Y.; Wang, J.-P.; Fang, H.-H.; Loi, M. A.; Zhao, N.; Wong, C.-P. Benzylamine-Treated Wide-Bandgap Perovskite with High Thermal-Photostability and Photovoltaic Performance. *Adv. Energy Mater.* **2017**, *7*, 1701048.

(43) Zhu, H.; Liu, Y.; Eickemeyer, F. T.; Pan, L.; Ren, D.; Ruiz-Preciado, M. A.; Carlsen, B.; Yang, B.; Dong, X.; Wang, Z.; et al. Tailored Amphiphilic Molecular Mitigators for Stable Perovskite Solar Cells with 23.5% Efficiency. *Adv. Mater.* **2020**, *32*, 1907757.

(44) Jiang, Q.; Zhao, Y.; Zhang, X.; Yang, X.; Chen, Y.; Chu, Z.; Ye, Q.; Li, X.; Yin, Z.; You, J. Surface Passivation of Perovskite Film for Efficient Solar Cells. *Nat. Photonics* **2019**, *13*, 460−466.

(45) Lai, X.; Meng, F.; Zhang, Q.; Wang, K.; Li, G.; Wen, Y.; Ma, H.; Li, W.; Li, X.; Kyaw, A.; Wang, K.; Sun, X.; Du, M.; Guo, X.; Wang, J.; Huang, W. A Bifunctional Saddle-Shaped Small Molecule as a Dopant-Free Hole Transporting Material and Interfacial Layer for Efficient and Stable Perovskite Solar Cells. *Sol. RRL.* **2019**, *3*, 1900011.

(46) Rajagopal, A.; Yao, K.; Jen, A. Toward Perovskite Solar Cell Commercialization: A Perspective and Research Roadmap Based on Interfacial Engineering. *Adv. Mater.* **2018**, *30*, 1800455.

(47) Chen, W.; Xu, L.; Feng, X.; Jie, J.; He, Z. Metal Acetylacetonate Series in Interface Engineering for Full Low-Temperature-Processed, High-Performance, and Stable Planar Perovskite Solar Cells with Conversion Efficiency over 16% on 1 cm^2 Scale. *Adv. Mater.* **2017**, *29*, 1603923.

(48) Luo, D.; Su, R.; Zhang, W.; Gong, Q.; Zhu, R. Minimizing Non-radiative Recombination Losses in Perovskite Solar Cells. *Nat. Rev. Mater.* **2020**, *5*, 44−60.

(49) Wang, H.; Yang, F.; Li, N.; Kamarudin, M.; Qu, J.; Song, J.; Hayase, S.; Brabec, C. Efficient Surface Passivation and Electron Transport Enable Low-Temperature Processed Inverted Perovskite Solar Cells with Efficiency over 20%. *ACS Sustainable Chem. Eng.* **2020**, *8*, 8848−8856.

(50) Wang, T.; Cheng, Z.; Zhou, Y.; Liu, H.; Shen, W. Highly Efficient and Stable Perovskite Solar Cells Via Bilateral Passivation Layers. *J. Mater. Chem. A* **2019**, *7*, 21730−21739.

(51) Wu, T.; Wang, Y.; Li, X.; Wu, Y.; Meng, X.; Cui, D.; Yang, X.; Han, L. Efficient Defect Passivation for Perovskite Solar Cells by Controlling the Electron Density Distribution of Donor-π-Acceptor Molecules. *Adv. Energy Mater.* **2019**, *9*, 1803766.

(52) Min, H.; Kim, G.; Paik, M. J.; Lee, S.; Yang, W. S.; Jung, M.; Seok, S. I. Stabilization of Precursor Solution and Perovskite Layer by Addition of Sulfur. *Adv. Energy Mater.* **2019**, *9*, 1803476.

(53) Anaraki, E. H.; Kermanpur, A.; Steier, L.; Domanski, K.; Matsui, T.; Tress, W.; Saliba, M.; Abate, A.; Grätzel, M.; Hagfeldt, A.; Correa-Baena, J.-P. Highly Efficient and Stable Planar Perovskite Solar Cells by Solution-processed Tin Oxide. *Energy Environ. Sci.* **2016**, *9*, 3128−3134.

(54) Chen, Z.; Turedi, B.; Alsalloum, A. Y.; Yang, C.; Zheng, X.; Gereige, I.; AlSaggaf, A.; Mohammed, O. F.; Bakr, O. M. Single-Crystal $MAPbI_3$ Perovskite Solar Cells Exceeding 21% Power Conversion Efficiency. *ACS Energy Lett.* **2019**, *4*, 1258−1259.